Pacific Graphics 2014
J. Keyser, Y. J. Kim, and P. Wonka
(Guest Editors)

Volume 33 (2014), Number 7

Single-shot High Dynamic Range Imaging Using Coded Electronic Shutter

Hojin Cho[1] Seon Joo Kim[2] Seungyong Lee[1]

[1]POSTECH [2]Yonsei University

Abstract

Typical high dynamic range (HDR) imaging approaches based on multiple images have difficulties in handling moving objects and camera shakes, suffering from the ghosting effect and the loss of sharpness in the output HDR image. While there exist a variety of solutions for resolving such limitations, most of the existing algorithms are susceptible to complex motions, saturation, and occlusions. In this paper, we propose an HDR imaging approach using the coded electronic shutter which can capture a scene with row-wise varying exposures in a single image. Our approach enables a direct extension of the dynamic range of the captured image without using multiple images, by photometrically calibrating rows with different exposures. Due to the concurrent capture of multiple exposures, misalignments of moving objects are naturally avoided with significant reduction in the ghosting effect. To handle the issues with under-/over-exposure, noise, and blurs, we present a coherent HDR imaging process where the problems are resolved one by one at each step. Experimental results with real photographs, captured using a coded electronic shutter, demonstrate that our method produces a high quality HDR images without the ghosting and blur artifacts.

Categories and Subject Descriptors (according to ACM CCS): I.3.3 [Computer Graphics]: Picture/Image Generation—Display algorithms I.4.3 [Image Processing and Computer Vision]: Enhancement—Sharpening and deblurring

1. Introduction

Real world scenes usually contain a wide range of brightness variations. When a scene consists of both bright and dark areas, ordinary low dynamic range (LDR) imaging devices, such as standard digital cameras, cannot capture the whole range of the scene radiance, losing expressive details in under-/over-exposed areas. This limited dynamic range of typical imaging devices has motivated various solutions for high dynamic range (HDR) imaging.

The most common HDR approach is to take multiple LDR images at different exposure levels and combine them to create an HDR image [DM97, MN99]. Despite significant advances, this approach assumes a constant radiance value per pixel among multiple images, and therefore works the best for static scenes without object motions and camera shakes. For dynamic scenes, the assumption of constant radiance value is violated, and the output HDR image would have artifacts such as ghosting and blurring. Object motions cause misalignments among multiple images which produces ghosting artifacts, and camera shakes under longer exposures induce motion blurs, reducing image sharpness. Such object motions and camera shakes are common in practice, and therefore removing these artifacts becomes crucial for successful HDR imaging.

The ghosting artifacts can be mitigated by either aligning the input images before combining them [KUWS03, MG10, ZBW11] or deghosting the output HDR image [ZC12, SL12, SKY*12, HGPS13]. However, aligning input images taken at different exposures is a difficult task, and most of deghosting methods are not robust against large object motions. For blur artifacts, a recent work employs image deblurring techniques in HDR imaging process [LHW*09], but it cannot handle object motion blurs. Special camera hardwares, such as multiple image detectors/sensor-elements, have been proposed for HDR imaging [NB03, TKTS11, WLA*12, MRK*13]. However, most hardware-based methods sacrifice spatial resolution for HDR imaging.

To overcome these limitations, we present a new single-shot HDR imaging method that utilizes a coded electronic shutter (CES). Recently an electronic shutter [Kod03] has

been widely adopted in digital cameras, and a CES can be implemented on top of the electronic shutter by triggering row-wise different signals (e.g., [MKS*05]) to obtain multiple exposures in a single image. To produce an HDR image, our approach exploits the row-wise multiple exposures obtained using a CES. As different exposures are simultaneously captured with the CES, ghosting effect is naturally avoided in the final HDR image. However, blur artifacts can still remain in the pixels of relatively longer exposure, so we present a novel motion blur removal algorithm to generate a sharp HDR image.

Our approach can be considered similar to a few previous methods [NB03, GHMN10] in the sense that spatially varying exposures are used. The most important difference is that our approach does not extract subimages with different exposures, while the previous methods [NB03, GHMN10] are based on such subimages obtained by interpolation. Our method directly extends the dynamic range through photometric calibration and image filtering algorithms, applied to the full-resolution image without sacrificing the spatial resolution. As a result, our approach does not suffer from jaggy artifacts caused by the interpolation, and preserves more fine-details than the previous methods. Experimental results show that our method produces high quality HDR images using an off-the-shelf camera equipped with a CES.

Our main contributions are summarized as follows.

- A novel approach to HDR imaging based on a Coded Electronic Shutter
- A robust framework for CES based HDR imaging, which avoids extraction of subimages for different exposures, preserving fine image details without jaggy artifacts
- A motion blur removal algorithm that eliminates the blurs and recovers image sharpness for long-exposure rows

2. Related work

Multiple image based approaches The most popular HDR imaging approach is to combine multiple LDR images captured at different exposure levels [DM97, MN99]. The radiometric response function for a camera is recovered using differently exposed images, and the image pixel value is converted to the radiance value through the computed response function. The state-of-the-art method in this category employs a unified HDR reconstruction pipeline from multi-sensor and multi-exposure images [KGBU13]. However, these methods assume constant radiance values in multiple images and therefore have limitations in handling dynamic scenes, especially when a target scene contains moving objects and is taken with a handheld camera.

Handling motion artifacts Object and camera motions produce ghosting and blur artifacts in the output HDR image, respectively. As ghosting artifacts are mainly caused by misalignments among multiple images, an intuitive solution is to align the input images before combining them to produce an HDR image. Simple approaches assume a planar and rigid scene, and solve for translational motions among images [TM07, Yao11]. However, real camera motions (e.g., rotations) are more complex than translations in many cases. More advanced solutions employ an optical flow based image registration [BM04] to handle nonuniform motions [KUWS03, MG10, ZBW11]. Despite the improvement in the results, such registration based approaches do not work robustly with saturations and occlusions.

Another approach for deghosting is to selectively combine a subset of exposures while rejecting the others that are misaligned by motions [ZC12,SL12,SKY*12,HGPS13]. However, most deghosting methods only work for the scenes with small motions because the radiance of a pixel is assumed to come from the same scene location over all exposures. The state-of-the-art approaches [SKY*12, HGPS13] could handle large motions and saturations, but they tend to produce blurry results as motion blurs are not explicitly handled. Although deghosting approaches are known as producing fewer artifacts than the registration based methods, their computation cost is relatively high. Thorough reviews on deghosting methods can be found in [SS12].

To address the blur artifacts, a recent work adopts image deblurring techniques in HDR imaging [LHW*09]. However, due to the dependency on the camera blur model, this approach can handle only global camera motion blurs, but not object motion blurs. Moreover, the iterative solution for image deblurring is often time consuming, and would not be applicable for HDR imaging on camera products.

HDR imaging hardware Special camera hardware devices have been proposed for HDR imaging, e.g., adaptive exposure control [NB03], light probe sequences [UGY07], beam splitter [TKTS11], optical add-on [MRK*13], and novel sensors that can capture HDR contents at a hardware level [WLA*12]. A main benefit of these devices is that they do not require the fusion of images with different exposures. However, most of them are not only difficult to be fabricated with high resolution, but also expensive as they are not commodity products yet.

A more cost-effective approach is to employ an exposure filter mask that accepts pixelwise different amounts of exposures [NM00, NN02, CAC*09, KMS09]. In this case, the misalignment problem (or ghosting artifacts) is naturally avoided since multiple exposures are captured simultaneously. These methods then extract subimages for different exposures, followed by a fusion step to generate an HDR image. However, this approach fundamentally suffers from a lack of spatial resolution and jaggy artifacts, which arise from the pixel value interpolation used to produce subimages. Recently another filter mask that exploits color channel sensitivities has been proposed [HS11], but its strong regularization shifts the tone of bright regions towards midtone.

The work that is closest to ours is the coded rolling shutter photography, proposed by Gu et al. [GHMN10]. Although

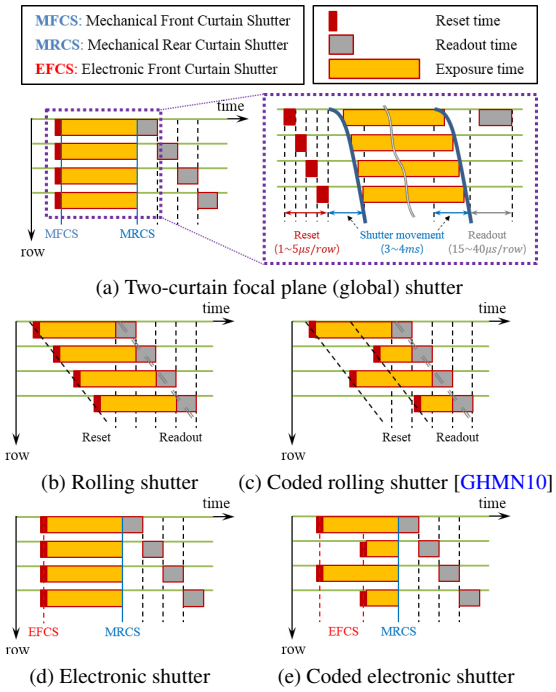

(a) Two-curtain focal plane (global) shutter

(b) Rolling shutter (c) Coded rolling shutter [GHMN10]

(d) Electronic shutter (e) Coded electronic shutter

Figure 1: *Conceptual timing charts for various camera shutters.*

the coded reset/readout signals [MKS*05] can provide multiple exposures within a single shot, this approach shares the same limitations to [NM00, NN02] because they first extract a subimage for each exposure using interpolation, which would produce jaggy artifacts in the final HDR image. Rolling shutters artifacts, such as skew and wobble, can also degrade the final image quality.

3. HDR Imaging Using Coded Electronic Shutter

3.1. Coded electronic shutter (CES)

Fig. 1 shows conceptual diagrams for different camera shutters. Fig. 1a illustrates the timing chart of a global shutter, commonly used in most of recent cameras. The two curtains determine the amount of incoming light by opening the front curtain and closing the rear one. Fast response (e.g., 3–4*ms*) is a major benefit of the global shutter, allowing all rows in the image sensor to acquire incoming light simultaneously.

In a rolling shutter camera, reset/readout signals replace the physical shutters (Fig. 1b). Unlike the global shutter, the rolling shutter operates sequentially since only one row can be signaled and activated at a time. The exposure is generally aligned with the readout because its time (e.g., 55.8-148.8*ms*) is longer than the reset time (e.g., 3.7–18.6*ms*) as

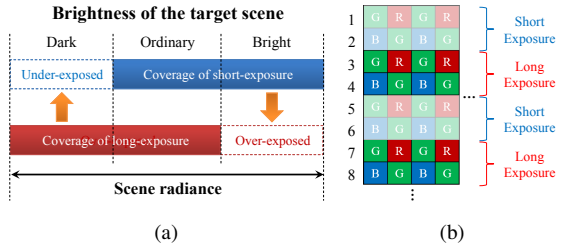

(a) (b)

Figure 2: *HDR imaging using a CES. (a) dynamic range extension using differently exposed pixels in a complementing way. (b) color filter array with row-wise varying exposures.*

illustrated in Fig. 1b†. Gu et al. [GHMN10] proposed an HDR imaging method using a coded rolling shutter (Fig. 1c) by adjusting the reset signals in the rolling shutter, similar to [MKS*05]. However, a rolling shutter and its variants necessarily involve spatial latency between rows due to the non-overlapping nature of signals (see Figs. 1b and 1c), producing undesirable skews and wobbles so called the rolling shutter distortion.

In this paper, we address the limitation by proposing a novel HDR imaging method based on a CES. The CES is based on the electronic shutter (e.g., [Kod03]), of which only the front curtain shutter of the global shutter is replaced by the reset signal while preserving the rear curtain shutter (Fig. 1d). Similar to [GHMN10], a CES can easily be implemented to simultaneously obtain row-wise varying exposures in a single image (Fig. 1e). But, we do not need to align exposure to the readout signals due to the fast physical rear shutter which prevents spatial latency between rows. Combining the merits of previous shutters, our approach based on CES does not suffer from rolling shutter distortion while allowing the concurrent capture of multiple exposures.

3.2. Basic idea and challenges

Our input image consists of two different exposures at $\pm s$ stop (or exposure value; EV) apart from a user-selected exposure, usually indicated as the shutter speed in the camera setting. The EV spacing s is a user parameter that determines the range of dynamic range extension. The dynamic range of an ordinary image is usually defined as $20\log(I_{max}/I_{min})$, where I_{max} and I_{min} are pixel intensities corresponding to the maximum and minimum radiance values, respectively. After compensating the gap between different exposures of the input (i.e., $2s$ EV), I_{max} will be increased by 2^{2s} because 1 EV corresponds to a standard power-of-2 exposure step and the output of a digital image sensor is linearly proportional to the exposure [VFTB97, Kor]. Thus, our output HDR image will

† Reset and readout signals take 1–5μs and 15–40μs for each row in an image, respectively, and we use an image of 5632×3720 pixels.

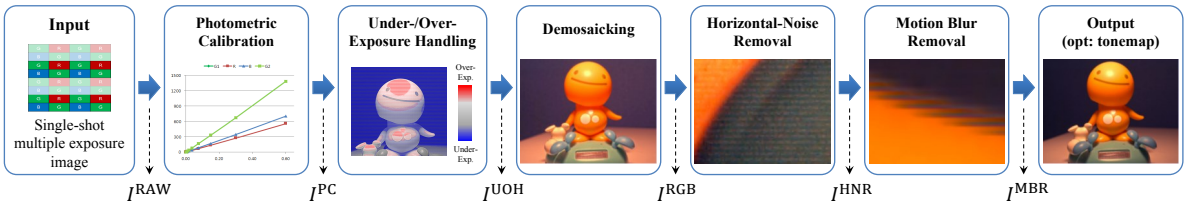

Figure 3: *Overall process of our HDR imaging using CES.*

have an extended dynamic range of $20\log(I_{max}/I_{min} \times 2^{2s})$ in the ideal case if we neglect the image noise.

Considering the 2×2 Bayer color filter array, the input image is modeled as

$$I^{\mathrm{RAW}} = \begin{cases} I_S & \text{on } 4n+1, 4n+2\text{-th rows} \\ I_L & \text{on } 4n+3, 4n+4\text{-th rows} \end{cases}, \quad (1)$$

where I_S and I_L are the short-/long-exposure images at $-s$ EV and $+s$ EV apart from the user-selected exposure, respectively, and $n = 0, 1, \cdots, \frac{\#rows}{4} - 1$. For notational simplicity, we use $I^{\mathrm{RAW}} = \{I_S, I_L\}$ to imply that subimages I_S and I_L are interlaced in a full image I^{RAW}. In our setting, I^{RAW} is a 12-bit image of 5632×3720 pixels, and its mosaic pattern is shown in Fig. 2b.

The key idea of our approach is to exploit multiple exposures in a single image acquired with a CES, and directly extend the dynamic range of I^{RAW} without separating I_S and I_L. Major benefits of our CES based HDR imaging system are that it prevents both the *spatial* latency (i.e., rolling shutter artifacts of [GHMN10]) and the *temporal* latency (i.e., ghosting by misalignments [DM97, MN99]).

To achieve high quality HDR imaging under this setting, a few challenging issues should be resolved:

- *Calibration of different exposures*: Since I_S and I_L in the input I^{RAW} have been obtained with different exposures (Fig. 4a), they should be calibrated into a single exposure before they are combined to extend the dynamic range.
- *Restoration of under-/over-exposed pixels*: With short-/long-exposures, I_S and I_L may contain under-/over-exposed pixels, which can produce color artifacts (Fig. 4b). These under-/over-exposed pixels should be restored using the nearby long-/short-exposure pixels (Fig. 2).
- *Compensation of different noise levels*: Since shorter exposure usually contains more noise, the noise levels of I_S and I_L are different, resulting in noticeable horizontal artifacts in the exposure-calibrated image (Fig. 4c), which should be corrected.
- *Removal of potential motion blurs*: With a longer exposure time, I_L may contain longer motions (i.e., larger blurs) than I_S when a dynamic scene is captured. The different amounts of blurs among I_S and I_L would appear as interlaced artifacts around object edges (Fig. 4d) and should be removed.

3.3. Our solutions

The overall process of our HDR imaging algorithm is illustrated in Fig. 3, which consists of several components to resolve the challenges mentioned in the previous section.

Photometric calibration: To calibrate the different exposure levels of I_S and I_L, we compute and utilize the response curve of the *image sensor* (Section 4.1). Note that since we are accessing the camera RAW images, estimating the radiometric response function as in [DM97] is unnecessary in our work. Instead, we compute the linear response of the image sensor that allows direct and effective conversion between raw pixel values with different exposures.

Under-/over-exposure handling: Given the single exposure obtained by photometric calibration, we restore the under-/over-exposed pixels using their well-exposed adjacent pixels while rejecting inaccurate ones. We present an effective bilateral filter that considers the pixel distance and the edge direction (Section 4.2).

Horizontal noise difference correction: To compensate the noise level difference between I_S and I_L, we analyze the property of the difference and utilize it to select an appropriate denoising method (Section 4.3).

Motion blur removal: Explicitly detecting and removing interlaced blur artifacts is difficult. We adapt a video deinterlacing method using the mean curvature flow [LS11], and extend it with an effective sharpness recovery step to avoid oversmoothing (Section 4.4).

4. Algorithm Details

This section describes each algorithmic component of Fig. 3 in detail with a real example in Fig. 4.

4.1. Photometric calibration

To compensate the different exposures in $I^{\mathrm{RAW}} = \{I_S, I_L\}$, the first step exploits the linear response assumption for digital image sensors [VFTB97, Kor], which implies that the sensor output is linearly proportional to the exposure. We validated the assumption experimentally for our image sensor. Fixing the ISO and aperture values, we took a static white panel in a controlled-light room (i.e., 0.15 lux) with

(a) I^{RAW} (b) I^{PC} in Section 4.1 (c) I^{UOH} in Section 4.2 (d) I^{HNR} in Section 4.3 (e) I^{MBR} in Section 4.4

Figure 4: *Intermediate results of our HDR imaging process. (a) input image taken with a handheld camera equipped with a CES. (b)-(d) intermediate results of the algorithmic components. For visualization, demosaicking and tone mapping have been used for (a)-(e).*

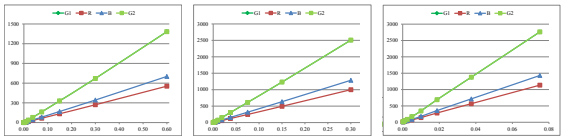

(a) ISO 200 (b) ISO 800 (c) ISO 3200

Figure 5: *Response curves of our CMOS image sensor: exposure (x-axis) vs. averaged raw pixel value on color filter array (y-axis). The exposure has been determined by controlling the shutter speed.*

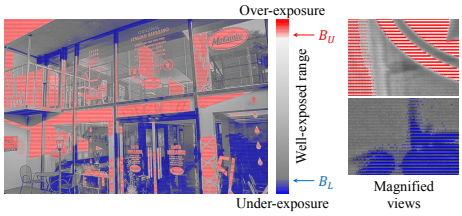

Figure 6: *Visualization of the over-exposed areas (red) and under-exposed areas (blue). Well-exposed areas are shown in gray.*

varying exposure time. We then determined the functional relationship between exposures and raw pixel values (i.e., sensor response) using the reciprocity [DM97], which implies that the optical density is determined by the product of the sensor irradiance and the exposure time. We conducted the experiments for seven ISO values from 100 to 6400 with the aperture value of $f/2$ and computed the sensor response by averaging about 3.5 million raw pixel values. As illustrated in Fig. 5, we observed that the response curve of our sensor is linear regardless of color channels and camera parameters.

With the linear sensor response, we compensate for the different exposures in I^{RAW} as follows.

1. Regress each response curve as $I = aE + b$, solving for constants a and b, where I and E represent the pixel and exposure values, respectively.
2. For the short exposure pixels I_S, compute their corresponding exposure values E_S using the inverse of the regression curve obtained in Step 1.
3. Compute the expected long exposure $E_{S\to L}$ by multiplying E_S and the ratio between exposure times of I_L and I_S.
4. Compute $I_{S\to L}$ from $E_{S\to L}$ using the regression curve.

Through the above steps, we obtain a calibrated long exposure image $I^{\mathrm{PC}} = \{I_{S\to L}, I_L\}$, as an update of I^{RAW}. The pixel values of I^{PC} have a $12+2s$ bit representation, where $2s$ is the exposure level difference between I_L and I_S. Fig. 4b shows an example of I^{PC}.

4.2. Under-/over-exposure handling

Although I^{PC} now has a uniform long exposure, it can contain under-/over-exposed pixels whose values are not reliable. For example, the red pixels inside the white object of Fig. 4b result from the saturation. White balancing on the saturated pixels in our image sensor increases the red pixel values because its red channel is less sensitive than the green and the blue.

Since the under-/over-exposed pixels themselves do not have accurate values, we have to utilize their well-exposed neighbors. Inspired by the edge dependent interpolation (EDI) algorithm for video deinterlacing [DHB98], we propose an effective bilateral filter that contains spatial weight w_s and edge-directional weight w_d:

$$I^{\mathrm{UOH}}(x) = \frac{1}{N} \sum_{y\in\Omega(x)} w_s \cdot w_d \cdot v(I(y)) \cdot I(y), \qquad (2)$$

where $I = I^{\mathrm{PC}}$ for notational simplicity, N is the sum of weights for normalization, x and y are indices for the under-/over-exposed pixel and its neighborhood in the same color channel, respectively, and Ω is a set of neighboring pixels just above or below the current row and within the radius of 3 centered at x in the Bayer color filter array.

The under-/over-exposed pixels are detected on I^{RAW} in advance using user-specified threshold values ($B_L = 2^5$ and $B_U = 2^{12} - 1 - B_L$), which correspond to the lower and upper bounds of the well-exposed range for our 12-bit input

image (Fig. 6). The validation function $v(\cdot)$ is defined as

$$v(I(y)) = \begin{cases} 1 & \text{if } I(y) > I(x) \;\&\; I^{\mathrm{RAW}}(x) > B_U, \\ 1 & \text{if } I(y) < I(x) \;\&\; I^{\mathrm{RAW}}(x) < B_L, \\ 0 & \text{otherwise.} \end{cases} \quad (3)$$

For an over-exposure pixel x, we can assume its pixel value $I(x)$ has been truncated due to the saturation, thus only neighboring pixels y whose values $I(y)$ are larger than $I(x)$ should be used to update $I(x)$. Note that the over-exposure handling is meaningful only for the pixels in the long-exposure rows I_L using the nearby pixel values in $I_{S\to L}$ (Fig. 2). If a short-exposure pixel in $I_{S\to L}$ is over-exposed, nearby long-exposure pixels would also be over-exposed, and there is no information we can use for recovering the over-exposed pixels. In this case, both the short- and long-exposed pixels remain unchanged. The symmetric argument also applies to the under-exposure handling.

In Eq. (2), w_s and w_d are respectively defined as

$$w_s = \exp^{-\frac{1}{2}(\|x-y\|/\sigma_s)^2}, \quad (4)$$

$$w_d = \exp^{-\frac{1}{2}(|\nabla^{\perp} I(x)\cdot \overrightarrow{xy}|/\sigma_d)^2}, \quad (5)$$

where $\nabla^{\perp} I(x)$ is the orthogonal direction to the image gradient at x, and $\overrightarrow{xy}$ is a direction vector from x to y. For experiments, we use $\sigma_s = 2$ and $\sigma_d = 0.1$, respectively. w_s penalizes the neighborhood far from x, and w_d gives more weights to the pixels whose orientation from x is similar to $\nabla I(x)$. Fig. 4c shows the result of under-/over-exposure handling.

4.3. Horizontal noise removal

After computing I^{UOH}, we apply an image demosaicking method [Ada97] to obtain a color image I^{RGB}, as illustrated in Fig. 3. The next step in the process is to correct for the different noise levels along horizontal lines in I^{RGB} caused by different exposure values.

In general, image noise is assumed to be additive Gaussian [BCM05]. Since the photometric calibration is just a linear transform of pixel values, we can expect the noise distribution of the calibrated pixels would also be Gaussian. However, the noise level of $I_{S\to L}$ differs from that of I_L because short exposures generally contain more noise and the noise in I_S is amplified in $I_{S\to L}$ through the photometric calibration. This amplified noise level of $I_{S\to L}$ gives rise to noticeable horizontal noise in I^{RGB} especially inside smooth regions, although it may not be prominent in textured regions (Fig. 4c).

To analyze the property of the noise level difference, we measure $err = I_{S\to L} - I_L$ for each color channel. Using the white panel images used for the validation test in Section 4.1, we sampled about 10,000 pixels from $I_{S\to L}$ and I_L for each color channel. Fig. 7 shows the distributions of err, which have the Gaussian distribution shapes, as the difference between two Gaussian distributions is also Gaussian.

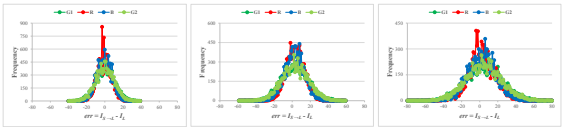

(a) 1/4s → 1/2s (b) 1/2s → 1/s (c) 1/4s → 1s

Figure 7: *Distributions of the noise level differences. We define the error as the difference between the calibrated pixel value and the ground truth at long exposure.*

The means of the distributions are almost zero, and the variance is most affected by the gap between exposure levels, where a larger gap gives a higher variance.

Based on this observation, we adapt a widely used denoising method, the bilateral filter [TM98], to remove the horizontal noise. The spatial kernel size is set as 5 or 7 pixels centered at the current pixel to include nearby pixels from both $I_{S\to L}$ and I_L. To prevent the different noise amounts among $I_{S\to L}$ and I_L from being considered as signal differences in bilateral filtering, we adjust the sigma (i.e., variance σ_r) for the range kernel according to the gap between exposure levels. In our implementation $\sigma_r = 0.03 \times 2^{12+2s}$. Fig. 4d shows the result of our horizontal noise removal step.

4.4. Motion blur removal

Since different exposure times have been used for I_S and I_L, motion blurs can appear as jaggy-like artifacts along the edges at object boundaries (Fig. 4d). It is hard to explicitly separate and remove such artifacts, so we adopt a mean curvature flow based video deinterlacing method [LS11] and extend it to better preserve the sharpness of the final output.

Blur artifact removal We begin with extending the image model in Eq. (1) as

$$I^{\mathrm{HNR}} = \begin{cases} I_{S\to L} \circ \Phi_S & \text{on } 4n+1, 4n+2\text{-th rows} \\ I_L \circ \Phi_L & \text{on } 4n+3, 4n+4\text{-th rows} \end{cases} \quad (6)$$

where I^{HNR} is the demosaicked intermediate result of Section 4.3, and Φ is a displacement vector field representing a relative pixelwise motion from the original pixel position. Although Φ does not exactly represent the motion blurs, it can handle blur artifacts resulting from expansions (or non-uniform displacements) of edge pixels. Without the loss of generality, we can represent Eq. (6) as $I^{\mathrm{HNR}} = I \circ \Phi$, omitting the subscripts.

To search for a smooth image from $\{I_{S\to L}, I_L\}$ minimizing the displacement Φ, Lenzen and Scherzer [LS11] proposed the following functional:

$$I^{\mathrm{MBR}} = \arg\min_I \int_\Omega \left[\frac{1}{2} \|\Phi(x) - x\|^2 + \alpha |\nabla I| \right] dx, \quad (7)$$

where α is the relative weight for total variation regularization $|\nabla I|$. $(\Phi(x) - x) = (\nabla I^T)^+ (I^{\mathrm{HNR}} - I)$ is the motion vector, so called the optical flow, and used for penalizing a

(a) Lenzen and Scherzer [LS11] (b) Our method

Figure 8: *Comparison of blur removal methods. (Left) output HDR image. (Right) gradient image. (b) preserves corners better than (a).*

large displacement. $^+$ denotes the Moore-Penrose pseudo-inverse. The semi-group solution of Eq. (7) is

$$I_t = |\nabla I|^2 \operatorname{div}\left(\frac{\nabla I}{|\nabla I|}\right), \tag{8}$$

where I satisfies Neumann boundary conditions. More details of the solution derivation can be found in [LS11]. Note that Eq. (8) is a kind of mean curvature flow with a different leading factor (i.e., $|\nabla I|^2$ instead of $|\nabla I|$). As demonstrated in Fig. 8a, applying Eq. (8) to I^{HNR} removes the blur artifacts effectively.

Sharpness recovery Since Eq. (8) can oversmooth the image, we extend the algorithm to preserve the sharpness. In Eq. (6), we can assume that $I_{S\to L}$ is not affected by the motion blur during the capture, because it is originally obtained at short exposure. Accordingly, Φ_S becomes reduced to a delta function, and we only have to consider Φ_L in Eq. (7). However, the mean curvature flow in Eq. (8) shrinks the whole image features such as corners and edges, as shown in Fig. 8a.

To overcome the limitation, we incorporate an effective sharpness recovery step into our motion blur removal by exploiting the sharpness information in $I_{S\to L}$ of I^{HNR}. Inspired by the feedback-control upsampling [SLJT08] and the back-projection method [IP93], which enforce the constraint from the input image during iterative image restoration, we substitute $I_{S\to L}$ for I^{MBR} at short exposure pixels. However, this may cause the mismatch of sharpness in adjacent rows reproducing jaggy-like artifacts, so the pixel-substituted image is passed to the next iteration. As a result, our algorithm preserves the details in $I_{S\to L}$ as much as possible, while aligning $I_L \circ \Phi_L$ to $I_{S\to L}$ via iterative refinement.

Algorithm 1 summarizes our detail-preserving motion blur removal process. In the algorithm, the parameters *#outer_iters* and *#evolutions* need to be adjusted according to the extent of blur, and in our implementation, we use $\#outer\_iters = 5$ and $\#evolutions = 15$. As shown in Fig. 8b, the proposed algorithm removes the blur artifacts effectively while preserving more details than the original dejittering method [LS11].

Algorithm 1 Detail-preserving motion blur removal

Input: I^{HNR}
Output: I^{MBR}
  $I^{\mathrm{MBR}} \leftarrow I^{\mathrm{HNR}}$ ▷ Initialization
  for $iter = 1 : \#outer\_iterations$ **do**
    for $t = 1 : \#evolutions$ **do** ▷ Blur artifacts removal
      $I^{\mathrm{MBR}} \leftarrow$ Compute Eq. (8) with $I = I^{\mathrm{MBR}}$
    end for
    for all $x \in I_{S\to L}$ of I^{HNR} **do**
      Substitute I^{MBR} with x ▷ Sharpness recovery
    end for
  end for

The final output I^{MBR} has the extended dynamic range of $12+2s$ bits. This output can be stored as a raw HDR image in the ".hdr" format. For visualization, we convert I^{MBR} into a smaller bit representation (e.g., standard 8-bit image) using the local adaptation tonemapper of Adobe Photoshop CS6. Fig. 4e shows the final output after the tone mapping.

5. Results

We implemented our method using C++. Our testing environment is a PC running MS Windows 7 with Intel Core i7 CPU and 12GB RAM. All the input images for our method were taken by a camera equipped with a CES. For other methods, multiple input images were obtained using the same camera by disabling the CES capability.

Fig. 9 shows a comparison with the most recent single-shot HDR imaging method [GHMN10] on a synthetic example. The synthetic raw image in Fig. 9b was obtained from the ground truth in Fig. 9a by sampling each color channel of the Bayer color filter array and adjusting the pixel intensities for rows to have relative shutter speeds $\{0.5s, 2s\}$. As shown in Fig. 9c, the method of [GHMN10] blurs fine details due to the extraction of subimages that involves image interpolation. Note that the interpolation was also used in [NM00, KMS09], thus they share the same limitation. The result of our method is shown in Fig. 9b, which preserves fine details and the sharpness better than [GHMN10]. We also measured the restoration errors quantitatively for comparing the two methods. The PSNR value of [GHMN10] is 26.07 dB, and that of our method is 27.73 dB.

Fig. 10 shows another comparison on a real example that contains many sharp features. To obtain the result of [GHMN10], we simulated the method using extracted subimages from our row-wise varying exposure image. As shown in Fig. 10a, [GHMN10] does not preserve horizontal line features. In contrast, our method better preserves horizontal lines and sharp features as shown in Fig. 10b.

Fig. 11 shows a comparison of various degrees of our dynamic range extension. Fig. 11a was taken with single exposure of {1/4s}. For Figs. 11b-e, we used the stop parameter

(a) Ground truth (b) Synthetic raw input (c) Gu et al. [GHMN10] (d) Our method

Figure 9: *Synthetic example. (b) is a grayscale image and visualized with colors for better representation. The PSNR value for (c) and (d) are 26.07 dB and 27.73 dB, respectively.*

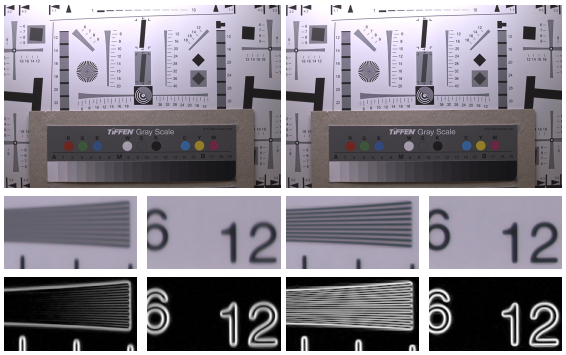

(a) Gu et al. [GHMN10] (b) Our method

Figure 10: *Comparison of recovered fine details with a real image of ISO 12233 resolution chart. The middle and bottom rows show the magnified views and their gradient image.*

$s = \{0.5, 1.0, 1.5, 2.0, 2.5\}$ for CES, given the indicated exposure of {1/4s}. With the parameters, our method produces diverse HDR images with different dynamic ranges.

Fig. 12 compares our method with multiple image based methods [DM97, HGPS13] for a dyanmic scene that contains moving objects of complex motions. Figs. 12a-b were produced from three images of shutter speed {1/125s, 1/60s, 1/30s}, using the implementation provided on internet by the authors. In Fig. 12a, the traditional method [DM97] suffers from ghosting artifacts around the moving dolls since it does not employ image registration or deghosting. In Fig. 12b, the state-of-the-art deghosting method [HGPS13] produces a high quality HDR image. However, [HGPS13] takes about 30 minutes to obtain a result at 1.7M pixels because of the repeated estimation of local homographies. In Fig. 12c, our method preserves fine image details and provides a comparable quality to [HGPS13]. However, our method takes less than five minutes to obtain a result at 20M pixels. Note that the previous method could not handle an image of large size due to the memory limit. Approximately, our method is 40 times faster than [HGPS13] under the same image resolution.

Fig. 13 shows additional results of real images from two stop to four stop extension. As shown in the result of four stop extension, our method can be applied to a very high dynamic range imaging. The supplementary material contains more comparisons and results including input images.

6. Discussion and Future Work

Row-wise exposure coding In our HDR imaging method, every two consecutive rows alternate between the short and the long exposures. This exposure sampling scheme complies the architecture of electronic shutter, while providing several advantages: (1) easy implementation as the reset and readout signals of the ordinary image sensor are activated row-wise, and (2) conformity to the vertical movement of the typical curtain shutter. Thus, the row-wise exposure sampling is a natural choice for the coded shutter in practice.

Spatial resolution and fine-details Although we sample row-wise varying exposures within a single image, we do not suffer from the reduction of spatial resolution as the pixel information is processed and combined in place rather than being separated into subimages (Figs. 9 and 10). This is a main benefit of our method, compared to the previous single image based approaches [NM00, CAC*09, KMS09, GHMN10] that extract a subimage for each exposure, resulting in the loss of fine details.

Limitations and future work A large gap between short- and long-exposure edges in the input image would require more iterations in Algorithm 1 while blur artifacts may not be completely removed. In addition, the bilateral filtering for horizontal noise removal could decrease image sharpness. Investigating more advanced deblurring and denoising methods would be important future work. Our algorithm with naive implementation takes about 3–5 minutes to produce an HDR image of 20 mega pixels. Although this is faster than

(a) Single exposure (b) 1 stop extension (b) 2 stop extension (c) 3 stop extension (d) 4 stop extension (e) 5 stop extension

Figure 11: *Our dynamic range extension results with real photographs. (a) Single exposure image taken with the shutter speed {1/4s}. (b)-(e) Our results with* $s = \{0.5, 1.0, 1.5, 2.0, 2.5\}$. *Magnified views in the bottom.*

(a) Debevec and Malik [DM97] (b) Hu et al. [HGPS13] (c) Our method

Figure 12: *Comparison with multiple image based methods when the scene contains moving objects. The first row illustrates the dynamic scene. The second row shows HDR image results. The last two rows show the magnified views.*

previous deghosting methods, it is not enough to be embedded inside a camera. Our future work includes accelerating the proposed method, and extending it for HDR video.

Acknowledgements

This work was supported by Basic Science Research Program of NRF (2012R1A1A2042837, 2013R1A1A2011692) and Samsung Electronics.

References

[Ada97] ADAMS JR. J. E.: Design of practical color filter array interpolation algorithms for digital cameras. In *Proc. SPIE 3028, Real-Time Imaging II, 117* (1997), pp. 117–125. 6

[BCM05] BUADES A., COLL B., MOREL J.: A review of image denoising algorithms, with a new one. *Multiscale Modeling & Simulation 4*, 2 (2005), 490–530. 6

[BM04] BAKER S., MATTHEWS I.: Lucas-kanade 20 years on: A unifying framework. *International Journal of Computer Vision (IJCV) 56*, 3 (2004), 221–255. 2

[CAC*09] CHENG C.-H., AU O., CHEUNG N.-M., LIU C.-H., YIP K.-Y.: High dynamic range image capturing by spatial varying exposed color filter array with specific demosaicking algorithm. In *Proc. IEEE Pacific Rim Conference on Communications, Computers and Signal Processing (PacRim), 2009* (2009), pp. 648–653. 2, 8

[DHB98] DE HAAN G., BELLERS E.: Deinterlacing-an overview. *Proceedings of the IEEE 86*, 9 (1998), 1839–1857. 5

[DM97] DEBEVEC P. E., MALIK J.: Recovering high dynamic range radiance maps from photographs. In *Proc. the 24th annual conference on Computer graphics and interactive techniques* (1997), SIGGRAPH '97, pp. 369–378. 1, 2, 4, 5, 8, 9

[GHMN10] GU J., HITOMI Y., MITSUNAGA T., NAYAR S.: Coded rolling shutter photography: Flexible space-time sampling. In *Proc. ICCP 2010* (2010), pp. 1–8. 2, 3, 4, 7, 8

[HGPS13] HU J., GALLO O., PULLI K., SUN X.: HDR deghosting: How to deal with saturation? In *Proc. CVPR 2013* (2013). 1, 2, 8, 9

[HS11] HIRAKAWA K., SIMON P.: Single-shot high dynamic range imaging with conventional camera hardware. In *Proc. ICCV 2011* (2011), pp. 1339–1346. 2

[IP93] IRANI M., PELEG S.: Motion analysis for image enhancement: Resolution, occlusion, and transparency. *Journal of Visual Communication and Image Representation 4*, 4 (1993), 324–335. 7

[KGBU13] KRONANDER J., GUSTAVSON S., BONNET G., UNGER J.: Unified HDR reconstruction from raw CFA data. In *Proc. ICCP 2013* (2013), pp. 1–9. 2

[KMS09] KONNIK M., MANYKIN E., STARIKOV S.: Optical-digital correlator with increased dynamic range using spatially varying pixels exposure technique. *Optical Memory and Neural Networks 18*, 2 (2009), 61–71. 2, 7, 8

[Kod03] KODAK: Shutter operations for ccd and cmos image sensors, December 2003. [Online; Application note, MTD/PS-0259]. 1, 3

[Kor] KOREN N.: Tonal quality and dynamic range in digital cameras. http://www.normankoren.com/digital_tonality.html. [Online; accessed 13-June-2014]. 3, 4

[KUWS03] KANG S. B., UYTTENDAELE M., WINDER S., SZELISKI R.: High dynamic range video. *ACM Trans. Graphics 22*, 3 (2003), 319–325. 1, 2

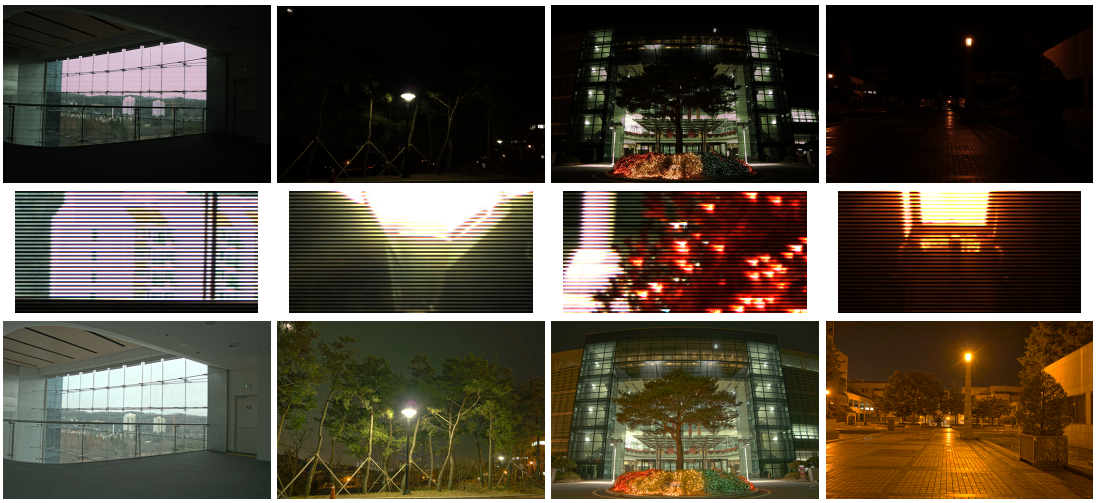

2 stop extension from 1/125s | 3 stop extension from 1s | 3 stop extension from 2s | 4 stop extension from 1s

Figure 13: *HDR imaging results. (top) Input multiple exposure images. (middle) Magnified views of the input. (bottom) Our HDR outputs.*

[LHW*09] LU P.-Y., HUANG T.-H., WU M.-S., CHENG Y.-T., CHUANG Y.-Y.: High dynamic range image reconstruction from hand-held cameras. In *Proc. CVPR 2009* (2009), pp. 509–516. 1, 2

[LS11] LENZEN F., SCHERZER O.: Partial differential equations for zooming, deinterlacing and dejittering. *International Journal of Computer Vision (IJCV) 92*, 2 (2011), 162–176. 4, 6, 7

[MG10] MANGIAT S., GIBSON J.: High dynamic range video with ghost removal. In *Proc. SPIE* (2010), vol. 7798, pp. 779812–779812–8. 1, 2

[MKS*05] MASE M., KAWAHITO S., SASAKI M., WAKAMORI Y., FURUTA M.: A wide dynamic range cmos image sensor with multiple exposure-time signal outputs and 12-bit column-parallel cyclic a/d converters. *IEEE Journal of Solid-State Circuits 40*, 12 (2005), 2787–2795. 2, 3

[MN99] MITSUNAGA T., NAYAR S.: Radiometric self calibration. In *Proc. CVPR 1999* (1999), vol. 1, pp. 374–380. 1, 2, 4

[MRK*13] MANAKOV A., RESTREPO J. F., KLEHM O., HEGEDÜS R., EISEMANN E., SEIDEL H.-P., IHRKE I.: A reconfigurable camera add-on for high dynamic range, multispectral, polarization, and light-field imaging. *ACM Trans. Graphics 32*, 4 (2013), 47:1–47:14. 1, 2

[NB03] NAYAR S., BRANZOI V.: Adaptive dynamic range imaging: optical control of pixel exposures over space and time. In *Proc. ICCV 2003* (2003), vol. 2, pp. 1168–1175. 1, 2

[NM00] NAYAR S., MITSUNAGA T.: High dynamic range imaging: spatially varying pixel exposures. In *Proc. CVPR 2000* (2000), vol. 1, pp. 472–479. 2, 3, 7, 8

[NN02] NAYAR S., NARASIMHAN S.: Assorted Pixels: Multi-Sampled Imaging With Structural Models. In *Proc. ECCV 2002* (2002), vol. IV, pp. 636–652. 2, 3

[SKY*12] SEN P., KALANTARI N. K., YAESOUBI M., DARABI S., GOLDMAN D. B., SHECHTMAN E.: Robust patch-based HDR reconstruction of dynamic scenes. *ACM Trans. Graphics 31*, 6 (2012), 203:1–203:11. 1, 2

[SL12] SILK S., LANG J.: High dynamic range image deghosting by fast approximate background modelling. *Computers & Graphics 36*, 8 (2012), 1060–1071. 1, 2

[SLJT08] SHAN Q., LI Z., JIA J., TANG C.-K.: Fast image/video upsampling. *ACM Trans. Graphics 27*, 5 (2008), 153:1–153:7. 7

[SS12] SRIKANTHA A., SIDIBE D.: Ghost detection and removal for high dynamic range images: Recent advances. *Signal Processing: Image Communication 27*, 6 (2012), 650–662. 2

[TKTS11] TOCCI M. D., KISER C., TOCCI N., SEN P.: A versatile HDR video production system. *ACM Trans. Graphics 30*, 4 (2011), 41:1–41:10. 1, 2

[TM98] TOMASI C., MANDUCHI R.: Bilateral filtering for gray and color images. In *Proc. ICCV 1998* (1998), pp. 839–846. 6

[TM07] TOMASZEWSKA A., MANTIUK R.: Image registration for multi-exposure high dynamic range image acquisition. In *International Conference in Central Europe on Computer Graphics and Visualization (WSCG)* (2007). 2

[UGY07] UNGER J., GUSTAVSON S., YNNERMAN A.: Spatially varying image based lighting by light probe sequences. *The Visual Computer 23*, 7 (2007), 453–465. 2

[VFTB97] VORA P. L., FARRELL J. E., TIETZ J. D., BRAINARD D. H.: *Digital color cameras – 1 – Response models*. Tech. Rep. HPL-97-53, Hewlett-Packard Laboratories, Palo Alto, CA, 1997. 3, 4

[WLA*12] WAN G., LI X., AGRANOV G., LEVOY M., HOROWITZ M.: Cmos image sensors with multi-bucket pixels for computational photography. *IEEE Journal of Solid-State Circuits 47*, 4 (2012), 1031–1042. 1, 2

[Yao11] YAO S.: Robust image registration for multiple exposure high dynamic range image synthesis. In *Proc. SPIE* (2011), vol. 7870, pp. 78700Q–78700Q–9. 2

[ZBW11] ZIMMER H., BRUHN A., WEICKERT J.: Freehand HDR imaging of moving scenes with simultaneous resolution enhancement. *Computer Graphics Forum 30*, 2 (2011), 405–414. 1, 2

[ZC12] ZHANG W., CHAM W.-K.: Gradient-directed multiexposure composition. *IEEE Trans. Image Processing 21*, 4 (2012), 2318–2323. 1, 2